Numerical Investigation of Three-Dimensional Flow Structure at a River Confluence

Shinjiro Miyawaki[1], George Constantinescu[1*], Gokhan Kirkil[1], Bruce Rhoads[2] and Alexander Sukhodolov[3]

[1]Department of Civil and Environmental Engineering & IIHR-Hydroscience and Engineering, The University of Iowa, IA 52242 U.S.A.

[2]Department of Geography, University of Illinois at Urbana-Champaign, Urbana, IL 61801, U.S.A.

[3]Department of Ecohydrology, Institute of Freshwater Ecology and Inland Fisheries, Müggelseedamm 310, D-12587 Berlin, Germany

ABSTRACT

Detached Eddy Simulation (DES) is performed to investigate the 3-D flow dynamics and the role of the large-scale coherent structures at an asymmetrical river confluence with concordant bed. The mean flow predictions are validated using data from a field study. The geometry of the confluence induces strong flow convergence and large-scale secondary circulation. DES is conducted at field conditions (average channel Reynolds number is 160,000). DES accurately predicts most of the large-scale features of the mean streamwise velocity distributions in cross-sections situated downstream of the junction. The present study demonstrates the important role played by the large-scale streamwise oriented vortices and associated helical motion in the momentum exchange processes between the two streams. It is shown the presence of these vortical cells on both sides of the shallow mixing layer developing downstream of the junction is responsible for some of the large-scale characteristics of the streamwise velocity distributions. DES results indicate that at the cross section within the scour hole downstream of the junction the streamwise-oriented vortical cell on the inner side of the mixing layer is larger and stronger than the one on the outer side of this layer. This effect is mainly due to the secondary circulation induced by the inner bank curvature and the realignment of the flow from the lateral tributaryas within the confluence region. The poor agreement of streamwise velocity distributions predicted by RANS with the field data is due to the underprediction of the strength of these cells of helical motion. Large-scale helical structures probably play an important role in shaping the bed in the downstream channel, as the bed friction velocity values beneath these cells are comparable to or higher than values below the mixing layer eddies.

INTRODUCTION

River confluences are common elements of river networks on all scales that are characterized by complex large-scale turbulent motions. Examples include a tributary merging with a larger stream or the joining of two branches of a braided river. Understanding the fluvial dynamics and mass exchange processes (sediment transport, contaminant transport, heat transfer, etc.) of stream confluences is

33rd IAHR Congress: Water Engineering for a Sustainable Environment

ISBN: 978-94-90365-01-1

important for predicting local effects, such as the development of scour holes and the mixing of converging streams. Confluences also play an important role in regulating the movement of sediment through braided river systems (Paola, 1997). Flow structure and patterns of scour downstream of the confluence are mainly affected by the momentum and velocity ratios between the two incoming streams, by the magnitude and ratio of the angles between the incoming streams, and by the flow direction downstream of the junction. The degree of concordance of the channel beds at the entrance to the confluence, the presence of a high channel curvature downstream of the junction, or of other large-scale spatial changes in the bed morphology around the confluence (e.g., large-scale bed features in the form of submerged dikes, bottom cavities or bank protrusions which induce separation) can further complicate flow patterns and the momentum and mass exchange processes.

While in the case of two incoming parallel streams, the mass and momentum exchange are controlled by the shallow mixing layer that forms downstream of the junction because of different velocities of the two streams, when the two incoming streams are not parallel (i.e., the case of direct relevance to river confluences), the flow dynamics is much more complex (Rhoads and Sukhodolov, 2008). Strong streamwise-oriented cells of helical motion are generally observed to form adjacent to the shallow mixing layer beneath the free surface (Rhoads and Kenworthy, 1995, 1998; Rhoads, 1996). The sizes and strengths of these cells can be much larger than the one of the predominantly vertical eddies that are convected inside the mixing layer. The mixing layer eddies are generated by Kelvin-Helmholtz instabilities and vortex pairing is responsible for their growth as they are convected downstream. The growth of the shallow mixing layer eddies is impeded by bed friction.

The mechanism responsible for the formation of the streamwise-oriented cells is directly controlled by the angle between the two incoming streams (junction angle of the confluence). As a result of the collision of the fluids from the two streams, the loss in kinetic energy associated with the decrease in the transverse velocity produces an increase of the pressure and a rise of the free surface in the vicinity of the region where the two streams collide (i.e. the upstream junction corner). This region roughly coincides with the upstream part of the mixing layer. The raised free surface elevation induces a vertical flow component oriented toward the bed inside the mixing layer. As this flow current approaches the bed, it is diverted away from the mixing layer on its both sides and then upwards back toward the free surface. As a result, a pair of counter-rotating vortices forms. Their axes are roughly parallel to the opposite sides of the mixing layer. The high-speed free-surface flow entrained into these streamwise-oriented cells is convected downstream, thus the fluid particles follow a helicoidal path. Secondary streamwise-oriented vortices situated in between the primary cells and the banks can also form.

These vortical structures play an important role in mass exchange processes. For example, sediment particles entrained at the bed beneath these vortices can be convected over large streamwise distances inside the core of these cells before being ejected back into the surrounding turbulent flow. The efficiency of this scour mechanism driven by the presence of strong streamwise-oriented vortical cells explains to a large extent the large dimensions of the scour holes observed to form downstream of confluences. The passage of the predominantly vertically oriented

mixing layer eddies provides a second mechanism for the growth of the scour hole. As will be shown by results of the present investigation, the first mechanism is stronger, at least for cases where the angle between the two incoming streams is relatively high. The strengths of these cells forming on each side of the mixing layer are mainly dependent on the angle between the incoming stream and the axis of the channel downstream of the junction. The asymmetrical confluence considered in the present study (incoming stream on the East side makes an angle of about 60^0 with the downstream channel) provides a good test case in which the role of these streamwise oriented vortical cells is expected to be significant.

As in most cases the resolution of the data obtained from field experiments is not fine enough to resolve all the dynamically important vortical structures and to capture all the relevant details of the flow, joint numerical and field studies can add to the general understanding of the physics of flow around river confluences. Because of the strong three-dimensionality of the flow and the important role played by large-scale coherent structures, eddy-resolving techniques have to be used in the numerical study to be able to capture the unsteady dynamics of these eddies and to understand how they affect the mean flow, bed shear stress distributions and turbulence statistics. In particular, these techniques can help elucidate the exact role played by the

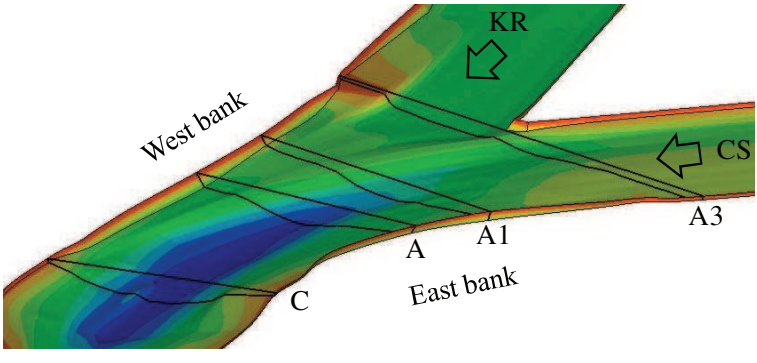

Figure 1. View of computational domain surrounding the confluence. The bathymetry is visualized using bed elevation contours.

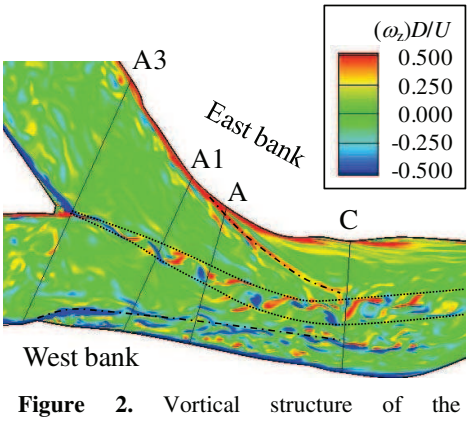

Figure 2. Vortical structure of the instantaneous flow at the free surface visualized using vertical vorticity contours

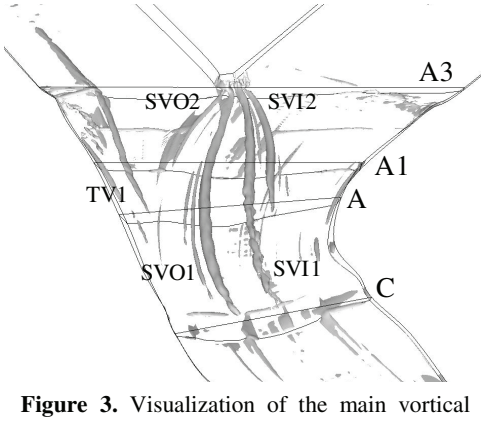

Figure 3. Visualization of the main vortical structures in the mean flow using the Q criterion.

streamwise-oriented cells of helical motion in confluence dynamics. Performing high-resolution simulations at comparable Reynolds numbers to those in the field experiments and being able to account for the presence of a rough channel bed adds to the relevance of the numerical study. Eddy-resolving numerical simulations provide 3D visualizations of the entire (averaged and instantaneous) flow field. This approach highlights the dynamics of the main coherent structures in the flow and the nature of their interactions with other coherent structures and with the bed. In the present paper we focus on the 3-D time-averaged (mean) flow structure.

NUMERICAL MODEL AND SIMULATION SET UP

Detached Eddy Simulation (DES) is a hybrid RANS-LES technique that is employed in the present study to simulate the flow at the confluence of Kakaskia River (West side of the confluence) and Copper Slough (East side) situated in east central Illinois, USA. The cross-section of both tributaries is trapezoidal. The flow and thermal mixing at this asymmetrical confluence (see Fig. 1) were already studied in a field experiment conducted by Rhoads and Sukhodolov (2001). Their data are used to validate the present DES model. The West side tributary is close to parallel to the downstream channel, while the East side tributary forms an angle of about 60^0 with the downstream channel. The channel beds of the two tributaries are concordant but a submerged block of failed bank material is present at the West (outer) bank close to the start of the junction. On the East side, the East (inner) bank curvature at the entrance into the downstream channel is high. The curvature radius of the channel nondimensionalized by the mean channel width is close to 3.5. This indicates that curvature-induced secondary currents may play an important role in determining the flow dynamics within and downstream of the confluence . The average mean flow velocity in the two tributaries $U=(U_W+U_E)/2= (0.42+0.46)/2$ is 0.44m/s. The average flow depth in the two channels upstream of the confluence is $D=(D_W+D_E)/2=(0.48+0.32)=0.4$m. This value is close to the average depth in the downstream channel, except for depths in the scour hole. The maximum scour depth in the scour hole is 2.92D and is recorded at a distance of about one and a half times the downstream-channel width from the upstream junction corner (Fig. 1). The corresponding Reynolds number is close to 166,000. The incoming discharges are $Q_W=1.41m^3/s$ and $Q_E=1.34m^3/s$, such that the momentum ratio $(\rho_W Q_W U_W)/ (\rho_E Q_E U_E)$ is close to unity (0.97). Thus, the development of the mixing layer is driven mainly by the difference in the directions of the two incoming streams rather than by a difference in momentum.

The bathymetry data used to generate the mesh was available from the same field study. The computational domain was meshed with 4.5 million cells. The wall normal grid spacing of the first row of cells off the bed and channel sidewalls was close to two wall units, which is sufficient to avoid the use of wall functions. Using information from the field study, the equivalent non-dimensional bed roughness was estimated to be close to 800 wall units.

A general description of the DES code is given in Chang et al. (2007). The 3D incompressible Navier-Stokes equations are integrated using a fully-implicit fractional-step method. The governing equations are transformed to generalized curvilinear coordinates on a non-staggered grid. Convective terms in the momentum

equations are discretized using the fifth-order accurate upwind biased scheme. All other terms in the momentum and pressure-Poisson equations are approximated using second-order central differences. The discrete momentum (predictor step) and turbulence model equations are integrated in pseudo-time using alternate direction implicit (ADI) approximate factorization scheme. In the present DES simulation, the Spalart-Allmaras (SA) one-equation model was used. Time integration is done using a double time-stepping algorithm and local time stepping is used to accelerate the convergence at each physical time step. The time discretization is second order accurate. To better assess the predictive abilities of DES, a RANS simulation was run on the same mesh using the same code and base turbulence model (SA).

At the two inflow sections, turbulent inflow conditions corresponding to fully-developed turbulent channel flow are applied. The velocity fields containing resolved turbulence from preliminary periodic channel simulations are stored in a file and then

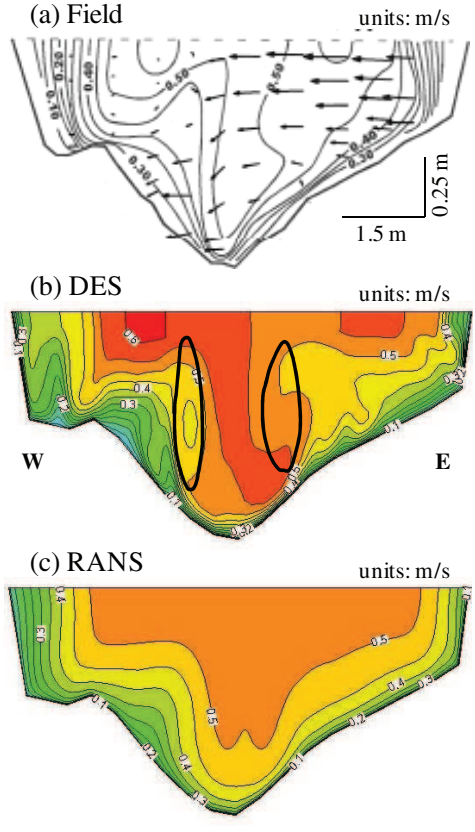

Figure 4. Mean streamwise velocity distribution in section A. a) field experiment; b) DES; c) RANS. The scale is distorted in the vertical direction (aspect ratio is 1:0.208). The two solid lines in frame b visualize the position of the main counter-rotating streamwise-oriented vortical cells.

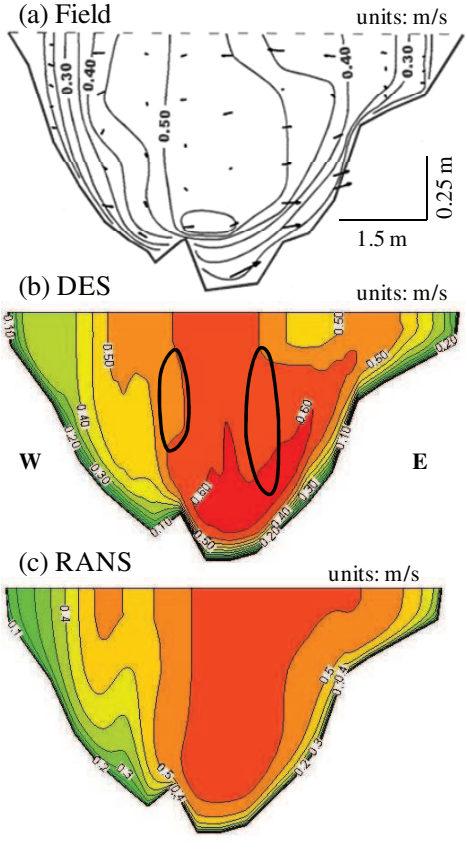

Figure 5. Mean streamwise velocity distribution in section C. a) field experiment; b) DES; c) RANS. The scale is distorted in the vertical direction (aspect ratio is 1:0.208). The two solid lines in frame b visualize the position of the main counter-rotating streamwise-oriented vortical cells

fed in a time-accurate manner through the inflow sections. At the outflow, a convective boundary condition is used. The free surface is treated as a rigid lid which is justified as the channel Froude number in the field experiment is 0.24. The walls are treated as rough no-slip boundaries.

RESULTS

The distribution of the instantaneous vertical vorticity in Fig. 2 visualizes the vortical structure of the flow at the free surface. The shedding and convection of strong vortical eddies inside the mixing layer in clearly captured. The average size of these eddies is growing as they are convected downstream. Velocity spectra confirm the fact that these eddies are quasi-two dimensional in the regions where their interactions with the other large-scale coherent structures is not significant. However, the vortical content of the flow is much more complex compared to the case of a shallow mixing layer developing in a very wide domain. Though the flow does not separate from the banks, the strong curvature of the East (inner) bank between sections A3 and C (see Fig. 1) induces the formation of a shear layer in which highly energetic vortical eddies are shed. The formation of a strong shear layer at the inner bank, especially in the regions situated close to the free surface, is a common feature of flow in bends of high curvature (Zeng et al., 2008). As shown in Fig. 2, these eddies intersect with the mixing interface around section C. Meanwhile, a region of shallow flow along the West bank, close to section A3, induces the formation of two shear layers, a predominantly vertical shear layer originating at its lateral extremity and a predominantly horizontal one originating at its crest. These two shear layers are similar to the ones observed to form as flow is advected past submerged dike-like structures (McCoy et al., 2007). Strong vortical eddies develop downstream of this location in between the high velocity core of the Kaskaskia River and the West bank. Most of these eddies originate in the horizontal shear layer that forms as fluid is advected over the top of the failed bank material near section A3. Past section A, these eddies start interacting with the mixing layer eddies. As shown in Fig. 2, by section C the eddies shed within the shear layers originating close to the two banks are as energetic as the vertically oriented eddies inside the mixing layer. Moreover, these eddies strongly disturb the mixing interface, interact and sometimes merge with the mixing layer eddies. The local flow structure is highly three-dimensional. Thus, the structure of the mixing layer developing downstream of section A is very different from the one expected in a wide stream in which interactions with large-scale turbulence originating at the banks is not significant.

At confluences characterized by a large junction angle, strong streamwise-oriented cells are expected to form on both sides of the mixing layer interface. Figure 3 uses the Q criterion to visualize the main vortical structures in the mean flow. Results confirm that the dominant vortical structures are two primary counter-rotating cells forming on the inner (SVI1) and outer (SVO1) sides of the mixing interface. Secondary elongated cells (SVI2 and SVO2) containing vorticity of the same sign to that in the primary cells are also present on both sides of the mixing interface. However, these secondary cells lose coherence rapidly and do not extend far downstream. Additionally, a tip vortex TV1 forms at the downstream end of the failed bank material, and a small vortex is present close to the inner (East) bank in the

region of high bank curvature. The magnitudes of the circulation of the two main streamwise-oriented vortices SVI1 and SVO1 are similar at section A1. The values are 0.9DU and 1.02DU, respectively. However, downstream of section A1 curvature induced effects amplify the strength of the streamwise oriented cells rotating counter-clockwise (SVI1 and SVI2) and decrease the strength of the cells rotating clockwise. Also, the level of interaction between the eddies shed from shear layers downstream of the submerged bank material and SVO1 is much larger than the level of interaction between the eddies shed from the shear layer along the inner bank and SVI1. These interactions strongly affect the cores of SVI1 and SVO1, contributing to their decrease in coherence downstream of section A. As a result of these phenomena, the magnitudes of the circulation of SVI1 and SVO1 are 1.36DU and 1.27DU at section A and 0.68DU and 0.46DU at section C, respectively. Moreover, SVO2 loses most of its coherence by section C. The coherence of the primary cells is significantly larger than that of the eddies convected inside the mixing layer interface. As discussed below, the growing imbalance between the strength of the primary cells on the two sides of the mixing interface has important consequences on the distribution of the streamwise velocity in cross sections situated at large distances from the upstream junction corner.

In agreement with the field data, the streamwise velocity distribution predicted by DES at section A shows the presence of two zones of maximum velocity at the free surface. These two zones are separated by a region of lower streamwise velocities. This is the typical pattern expected downstream of the junction between two tributaries. In fact, close to the upstream junction corner a recirculation (wake) region with negative streamwise velocities is present in both field data and DES. The wake region forms near the upstream junction corner in the region of stagnant flow (Rhoads and Sukhodolov, 2008). The primary counter-rotating streamwise-oriented vortices (the cores of these vortices are visualized in Fig. 4b) induce a strong downwelling of the flow within the mixing interface. As a result, some of the high velocity free-surface fluid is advected toward the bottom. At section A, DES predicts that the size of the region of high streamwise velocity on the outer (West) side is larger and the velocity magnitude slightly greater (by about 10-25%) than high-velocity core on the inner side of the section, in agreement with field measurements. Also, as a result of the position of the core of SVI1 and its interaction with the local bed topography, some of the high-velocity fluid convected by the action of the two helical cells near the bed within the interface is convected parallel to the bed beneath SVI1 and then upwards toward the surface. In contrast to DES, RANS does not capture the presence of two zones of high velocity in the section despite the fact that the primary counter-rotating helical cells are present in the solution. However, the coherence of these vortices (e.g., their circulation) in RANS is much smaller than that predicted by DES, so these vortices are not strong enough to significantly modify the regions of high-streamwise velocity within the section.

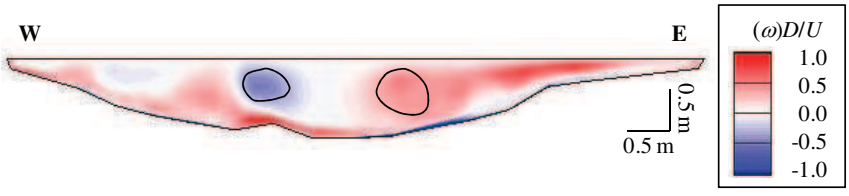

Figure 6. Distribution of streamwise-oriented vorticity in mean flow (DES) at section C.

In the downstream section C only one zone of maximum velocity is present. This zone is situated predominantly on the East side of the section. This is in contrast to results at upstream sections A3 to A where two zones of maximum velocity are observed. Part of the reason for the disappearance of the region of high velocity on the outer side of the section is related to the vortical structures present in the flow as a result of the submerged failed bank material (see Figs. 2 and 6). These eddies occupy most of the outer side of the section and their strength is comparable to that of the mixing layer eddies. Thus, flow within the mixing layer is strongly affected. In both DES and field experiment, the region of maximum streamwise velocity in section C is situated in the vicinity of the bed rather than the free surface and the position of this region is skewed toward the inner (East) side of the section. Similar to section A, two main counter-rotating helicoidal cells SVO1 and SVI1 are present. Curvature induced effects slow the rate of streamwise decay of the circulation of the counter-clockwise rotating vortex SVI1 and increase the rate of decay of the clockwise-rotating vortex SVO1. The larger velocities observed over the inner side of the section are a result of the convection of high velocity flow by the stronger vortex SVI1 first toward the inner bank along the bed and then upwards. SVI1 is not only stronger but also situated closer to the bed. This position increases its efficiency in entraining high velocity fluid from the central part of the section toward the inner bank. It also explains the irregular shape of the isovels corresponding to velocities of 0.5-0.55 m/s in the experiment and DES. By contrast, in the RANS results a small region of high velocity is still present at the outer (West) side of the section and the shapes of the isovels corresponding to streamwise velocity values of 0.5-0.55 m/s differ substantially from the measured ones. Also, RANS does not predict that the largest streamwise velocities are situated in the central part of the section close to the bed, a feature of the velocity distribution in section C captured by DES. This is again due to the failure of RANS to accurately predict the strength of helical motion on both sides of the section.

The distribution of the mean bed friction velocity in Fig. 7 implies that the cells of helical motion may play a determinant role in entrainment of sediment that contributes to the development of the scour hole. Moreover, these cells provide an effective mechanism for the transport of the sediment particles entrained from within the scour hole to large distances downstream of the scour hole. For the present configuration, the level of amplification of the bed friction velocity associated with quasi two-dimensional eddies in the mixing layer is less than the amplification beneath the two primary counter-rotating cells. Substantial amplification of the bed friction velocity is also observed beneath the secondary streamwise oriented cells SVI2 and SV02 between sections A3 and A1. The presence of a core of large streamwise velocity in the near bed region around the position of section C explains

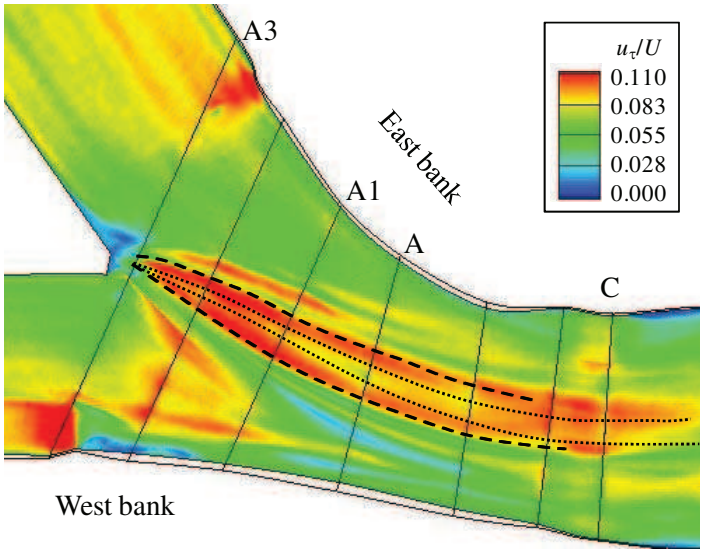

Figure 7. Distribution of the bed friction velocity u_τ/U in the mean flow. The dashed lines show the position of the cores of the primary counter-rotating streamwise-oriented vortices. The dotted lines show the position of the mixing layer.

the persistence of large bed friction velocity values in the central part of the downstream channel, at sections (e.g., around section C) situated in regions where a significant decay in the coherence of the primary cells of helicoidal motion is observed. The two patches of high bed friction velocity situated close to the two banks around section A3 correspond to the regions of flow acceleration where tributary flows are convected over topographic highs on the channel bed. The change from counter-rotating cells upstream to a dominant counterclockwise rotation downstream is also consistent with observed patterns of sediment sorting at this confluence for momentum ratio near one (Rhoads et al., in press).

C ONCLUSIONS

The three-dimensional structure of the time-averaged flow was analyzed at an asymmetrical river confluence with concordant bed. The use of eddy resolving techniques to compute the flow (DES) resulted in more accurate predictions of the mean streamwise velocity distributions compared to results from a steady RANS simulation. The present study demonstrates that coherent cells of helical motion associated with the formation of strong vortical eddies beneath the free surface on both sides of the mixing interface are a prominent feature of the flow structure at the confluence and are, to a large degree, responsible for the amplification of the bed friction velocity around the mixing interface. The strong curvature of the inner bank downstream of the upstream junction corner modifies the relative intensity of the primary counter-rotating cells. The circulation inside the cell on the inner (East) side decays at a slower rate than that of the cell on the outer (West) side. As a result, the typical streamwise velocity distribution containing two zones of high velocity on the two sides of the mixing interface, expected to be present at very wide confluences, is